Calculation of Nonlinear Subsonic Characteristics of Wings with Thickness and Camber at High Incidence

R. Gordon* and J. Rom†
Technion—Israel Institute of Technology, Haifa, Israel

A new vortex lattice model for the calculation of the flow over delta-shaped wing planforms at high angles of attack in subsonic flow is presented. This model enables the prediction of the aerodynamic coefficients and the pressure distributions for a wide range of wing planforms, in particular for delta-shaped wings with and without camber. The new vortex lattice model is combined with the panel source singularity for the calculation of the aerodynamic characteristics of thick wings having sharp leading edges. The calculated aerodynamic characteristics are in very good agreement with experimental data, while reasonable agreement is obtained in the evaluation of the pressure distributions. A parametric study of the numerical model and some numerical considerations which enable considerable reduction in computer time are also discussed.

Nomenclature

$\mathcal{R}$ = wing aspect ratio
$b(x)$ = wing local span
C_0 = wing root chord
$c(x,y)$ = wing mean camber function
C_D = drag coefficient
C_{D_i} = drag due to lift coefficient
C_L = lift coefficient
C_M = pitching moment coefficient taken about the wing apex
C_p = pressure coefficient
$f(x,y)$ = wing surface function
H = coefficient matrix calculated by the Biot-Savart law
N = number of cells or number of contributing line vortices
n = normal vector to the wing surface
NC = number of subdivisions of the root chord
NS = number of subdivisions of the semispan, $b/2$
R = ratio of leading-edge line vortex step length/wing-cell length = $\Delta x/\Delta h$
r = location vector
r_c = center of vorticity, Eq. (7)
t = maximum thickness of centerline airfoil section
$t(x,y)$ = wing thickness function
u,v,w = Cartesian components of perturbation velocity
V = velocity vector
$V_{\text{D.V.}}$ = velocity induced by local distributed vorticity vector
$V_{\text{L.V}}$ = velocity induced by line vortices
V_s = velocity induced by panel sources
x,y,z = Cartesian coordinates
X_{cp} = aerodynamic center of pressure
α = angle of attack
∇^2 = Laplacian operator
Δ = jump or change in a quantity
ΔC_p = $C_{p_{\text{lower}}} - C_{p_{\text{upper}}}$
Δh = wing cell length
Δx = step length
γ_0 = yawing angle measured with respect to wing symmetry plane
Γ = strength of a line vortex
$\boldsymbol{\Gamma}$ = vector of strengths of horseshoe line vortices
Λ = wing leading-edge sweep angle measured with respect to wing symmetric line
ϕ = perturbation potential
ρ = fluid density

Subscripts

c = center of vorticity
i = index of control point
j = index of station along a line vortex
n = normal to wing surface or wing mean camber surface direction
ref = reference quantity
∞ = freestream condition

Superscript

(i) = iteration number

Introduction

SLENDER pointed wings with highly swept sharp leading edges are of interest for both subsonic and supersonic flight. At subsonic flow conditions these wings develop separation-induced vortex flow at the incidences which occur in sharp maneuvers and at the takeoff and landing conditions. The flow separation takes the form of two free vortex layers joined to the leading edge of the wing, which roll up to form spiral-shaped vortex sheets above the wing. The low pressures associated with these vortices generate additional lift on the wing, thus causing the well-known nonlinear aerodynamic characteristics.

Potential flow methods that assume attached flow cannot predict accurately either the wing surface pressure distribution or the overall nonlinear aerodynamic coefficients of the wing.[1,2] Many theoretical methods have been developed to include the effects of the shed vortices. The leading-edge suction analogy method developed by Polhamus[1-4] predicts the aerodynamic coefficients C_L, C_D, and C_M reasonably well for delta wings with aspect ratio less than 2.0, but it does not provide the flowfield details or the surface pressure distributions. Theories based on slenderbody conical flow assumptions[5,6] qualitatively predict the observed pressure distribution over the front part of the wing but overpredict the experimental pressure distribution toward the trailing edge, thus providing inaccurate aerodynamic coefficients. Conical flow methods were followed by methods based on three-

Received March 18, 1983; revision received July 4, 1984.

*Research Fellow, Department of Aeronautical Engineering.
†Professor, Lady Davis Chair in Experimental Aerodynamics, Department of Aeronautical Engineering. Associate Fellow AIAA.

dimensional models in which the free vortex sheet is represented by a lattice of line vortices[7-15] or by vortex sheets.[16-20] These methods were reasonably successful in predicting the aerodynamic coefficients and in some cases also the pressure distributions for delta wings. A review of various methods based on rolling up vortex sheets for three-dimensional separation is presented in Ref. 21.

This paper presents a new vortex lattice method for the calculation of the flow over delta-wing planforms at high angles of attack. Results are obtained for a wide range of aspect ratios of flat delta wings. The new model is also applied to the calculation of the flow over a cambered delta wing. Results are obtained for a delta wing of $\mathcal{R}=1.15$ having a NACA 230 camber profile.

The new vortex model is combined with the panel source singularity for the calculation of the flow over thick wings. Results are obtained for a delta wing of $\mathcal{R}=1$ having a 12% thick biconvex profile. A parametric study of the method and some ways to reduce the computer time are also presented.

A compatible method of calculations of the aerodynamic characteristics of bodies at high angles of attack was presented by Almosnino and Rom.[35] These computation methods can be combined to enable the calculation of the aerodynamic characteristics of wing-body configurations up to relatively high angles of attack.

Method of Calculation

The perturbation velocity potential ϕ of the inviscid incompressible[‡] flow past a wing satisfies Laplace's equation:

$$\nabla^2\phi=0 \tag{1}$$

and the following boundary conditions: 1) the wing surface is impermeable, i.e., $(V_\infty+\nabla\phi)\cdot n=0$ on the wing surface; 2) there is no pressure jump across the wakes emanating from the leading edges and the trailing edges of the wing; 3) the Kutta condition which requires finite velocity at the wing trailing edges should be satisfied; 4) the disturbance velocity, $\nabla\phi$, must vanish far from the wing and the wake's surfaces.

The vortex lattice method for the solution of the problem posed above, for wing planforms of zero thickness is based on modeling the lifting surface by a system of horseshoe line vortices. These horseshoe line vortices emanate from the wing. The position of the separation location of these line vortices from the wing surface is specified by consideration of the physics of the flow separation over the wing. In the present method these vortices are allowed to separate at the trailing edges and at the side and leading edges of the wings, free to roll up, thereby simulating the wake and the free vortex sheets that separate from the sharp leading edges.

The method for the calculation of the flow over thick wings is based on modeling the wing thickness by potential panel sources of constant strength. The effects of camber, twist, and incidence are modeled by the superposition of a system of horseshoe line vortices as in the vortex lattice method. The details of the algorithm for the calculation of the aerodynamic characteristics of wings of zero thickness have been previously presented in Refs. 10 and 11. The Kutta condition is automatically satisfied for both the zero thickness case and the thick wing case by fulfilling the tangential flow boundary condition at the trailing-edge panels.

The relevant details for both thin and thick wings are included here in order to present a complete description of the general method for the thick wing calculations. A step-by-step description of the algorithm follows.

[‡]The problem can be extended to compressible subsonic flow by the application of the Prandtl-Glauert transformation.

Step A (for Thick Wings Only)

The wing surface function $f(x,y)$ is decomposed into the sum of two functions: $f(x,y)=c(x,y)\pm t(x,y)$. The wing thickness function, $z=\pm t(x,y)$ is set at zero angle of attack, and its chord plane is divided into a finite number of cells (panels). A control point is placed at the three-quarters point of the panel's root chord, on the center chord of each panel (Fig. 1). Sources of constant strength are distributed on each of the panels. The strength of the panel sources is determined by the solution of a system of linear equations set up to satisfy the boundary condition of tangential flow over the thickness configuration at the control points. The chord plane of the wing thickness configuration with the evaluated panel sources is now placed at the required angle of attack α.

The analytic expressions derived by Woodward[22] are used herein to calculate the perturbation velocity induced by the sources of constant strength distributed over the panels.

Step B

The mean camber surface of the wing is set at the required angle of attack α. Its chord plane is divided into a finite number of panels. A horseshoe line vortex is placed in each panel, with its bound vortex located at one quarter of the panel's chord, and a control point is located at three quarters of the middle chord of each panel (Fig. 2). The trailing vortices of the horseshoe line vortices emanate from the wing at its trailing edge or at its leading edges/side edges as prescribed.

Step C

The commonly used assumption according to which the free line vortices are straight lines in the x-z planes, leaving the wing edges at an angle $\alpha/2$ to the wing, is used in the present calculations.

Step D

An initial location of the free line vortices is assumed. The strength of the vortices is calculated by solving a system of linear equations set up to satisfy the boundary conditions of tangential flow over the camber surface of control points. The relation between the strengths of the line vortices and the normal vector of velocities at the control point is

$$H^{(i)}\cdot\Gamma_\alpha=-V_{\infty,n} \tag{2}$$

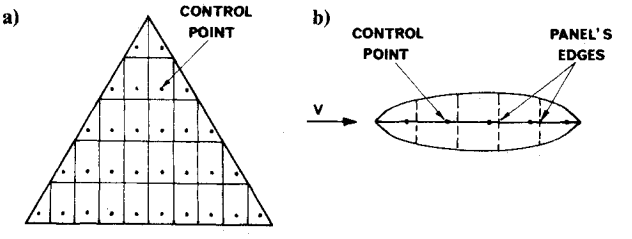

Fig. 1 Paneling of the chord plane of the thickness configuration: a) top view, b) side view at $y=0$.

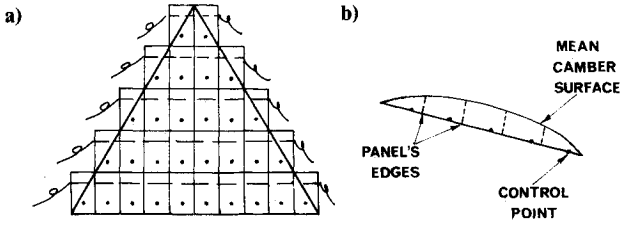

Fig. 2 Paneling of the chord plane of the mean camber surface: a) top view, b) side view at $y=0$.

where for thick cambered wings, $V_{\infty,n}$ is the freestream vector of velocities normal to the wing mean camber surface.

Step E

Now, the path of the free line vortices is updated by imposing the force free condition on the line vortices. The free line vortices are divided into a number of straight line segments followed by a semi-infinite line segment. The position of each line vortex is updated as follows: starting the calculation from the first point at the wing edge, each division point of the line vortex is updated until all points on the line are recomputed. The new position of each point is calculated from the latest positions of all the line vortice segments, including the newly calculated positions, according to

$$y_j^{(i)} = y_{j-1}^{(i)} + \frac{v_{j-1}^{(i)}}{V_\infty + u_{j-1}^{(i)}}(x_j - x_{j-1})$$

$$z_j^{(i)} = z_{j-1}^{(i)} + \frac{w_{j-1}^{(i)}}{V_\infty + u_{j-1}^{(i)}}(x_j - x_{j-1}) \qquad (3)$$

In the case of thick wings, the induced velocity components also include the velocity components induced by the panel sources that were calculated in Step A. This calculation is repeated for every line vortex that separates from the wing planform. Equations (3) are a numerical expression for the condition of force-free line vortices: $\rho \cdot V \times \Gamma = 0$.

Step F

The process is recycled by replacing the previous approximation of the free line vortices location by the new approximation and returning to step D. The process continues until a given convergence criterion for the position of the free line vortices is obtained. After the convergence of the calculations of the positions and strengths of the free line vortices has been achieved, the pressure coefficient at each control point on the wing chord plane is calculated. The forces and moments acting on the wing are then obtained by numerical integration, as described in the next section.

Calculation of Pressure Coefficient Distribution and Aerodynamic Coefficients of the Wing

The numerical calculation presented in the previous section yields the velocity field from which the pressure coefficients are calculated at the control points and then integrated to find the forces and moments acting on the wing.

The pressure coefficient is calculated by Bernoulli's equation

$$C_{p_i} = 1 - [(V_\infty + u_i)^2 + v_i^2 + w_i^2]/V_\infty^2 \qquad (4)$$

For thick wings the induced velocity at control point i is given by

$$V_i = V_{\text{L.V.},i} + \tfrac{1}{2} \cdot V_{\text{D.V.},i} + V_{s,i_{\text{upper}}}$$

on the upper surface and

$$V_i = V_{\text{L.V.},i} - \tfrac{1}{2} \cdot V_{\text{D.V.},i} + V_{s,i_{\text{lower}}} \qquad (5)$$

on the lower surface.

For wings with zero thickness, we obtain from these equations

$$\Delta C_{p_i} = 2 \cdot (V_\infty + V_{\text{L.V.},i}) \cdot V_{\text{D.V.},i}/V_\infty^2 \qquad (6)$$

The calculation of the velocity induced by the distributed vorticity vector at control point i is detailed in Ref. 23.

Delta-Wing Paneling

Chord Plane Paneling of Delta Wing Mean Camber Surface

The chord plane of the mean camber surface of delta wings is divided into panels by a new delta paneling method. In this method the chord plane is divided into panels by equally spaced spanwise lines and the same number of equally spaced chordwise lines as shown in Fig. 2. The triangular panels formed at the leading edge are extended outside the wing chord plane to form rectangular panels similar to the inner panels. A horseshoe line vortex is placed on each of these panels with its bound vortex located at the panel's one-quarter chord. A control point is placed at three quarters of the panel's center chord. The trailing line vortices of the inner panels' horseshoe line vortices are embedded in the wing chord plane and emanate from the wing at the trailing edge. The trailing line vortices at the leading edge are allowed to emanate from the wing into the freestream and are free to interact and roll up into the leading-edge vortex pattern.

The present method was found to give very good results in comparison with experimental data over a wide range of aspect ratios of delta wings. The shedding of line vortices at the leading edges of delta wings generates the nonlinear behavior of the aerodynamic characteristics at high angles of

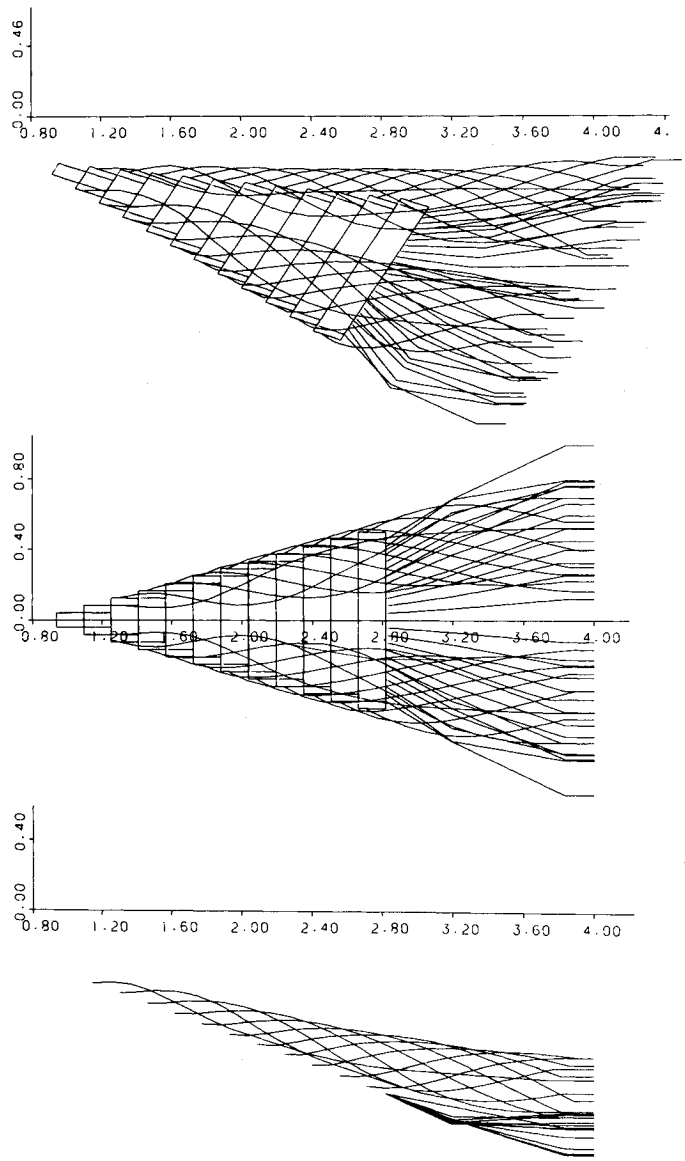

Fig. 3 The calculated wing and wake's shape for a flat planform delta wing of $A = 1$, for NC × NS = 12 × 12 at $\alpha = 20$ deg.

attack. The calculated aerodynamic characteristics of delta wings strongly depend on the strength of the line vortices shed at the leading edges. The strengths of these line vortices depend mainly on the geometry of the panels at the leading edge. The present method geometry of the leading-edge panels is responsible for the proper strengths of the leading-edge line vortices. Note that the extension of vortices of the leading-edge panels out of the wing has a different angle than that used in Refs. 13-15. It was found that for small aspect ratios the results obtained by the two models are similar, while the present model enables convergent results to higher aspect ratios of 2-3. In the forces and moments calculations, only the actual area in the leading-edge panels is taken into account.

For cambered wings the line vortices mesh is laid out on the wing chord plane. This ensures that the strength of the line vortices, especially the strength of the leading-edge line vortices would be free of the effect due to the surface curvature deformation at the leading-edge cells. It also ensures that in the case of thick, cambered wings, the control points of the thickness configuration coincide with the control points of the camber surface.

Chord Plane Paneling of the Thickness Configuration of Thick Delta Wings

The chord plane of the thickness configuration is divided into panels by the delta division method that was described in the previous section. The same number of subdivisions is used for paneling the chord plane of the thickness configuration and the chord plane of the mean camber surface of thick wings. Thus, for thick wings the control points on the chord plane of the thickness configuration coincide with the control points on the chord plane of the mean camber surface.

Reduction of Computing Time

Reduction of the computation time was achieved by 1) modifying the iterative procedure 2) a more efficient calculation of the induced velocities and 3) the use of a geometrical spacing for the free vortices in the wake.

The introduction of these changes (details are given in Ref. 23) resulted in reduction of the computer time by an order of magnitude to about 2-20 min on the IBM 370/168 computer.

Results and Discussion

Results for Flat Planform Delta Wings

Figure 3 shows the computed flowfield of the line vortices shed from flat-planform delta wing of $\mathcal{R}=1$ at $\alpha=20$ deg. The computed flowfield pattern agrees well with experimental visualization of the flowfield.[24] In the calculations, the first leading-edge line vortex closest to the wing apex tended to oscillate in space during the iterative process, thereby preventing a full convergence of the procedure. In order to prevent this, the first leading-edge line vortex was forcibly embedded in the wing plane, leaving the wing only at the trailing edge. In order to prevent numerical problems, a cutoff distance of $10^{-4}\ C_0$ is used in all present calculations.

Figure 4 shows the computed results for the lift coefficients and for the pitching moment coefficients, calculated for planform delta wings of $\mathcal{R}=0.25$, 0.5, 1.0, 2.0, at $\alpha=20$ deg. The results are compared with the computed results of Johnson et al.,[19] obtained by the Boeing-LEV code calculated once with a simple wake model and once with a near wake model. The results are compared also with the results of the suction analogy of Polhamus and with experimental data obtained from Refs. 25-30. The present results are calculated with $NC\times NS=12\times 12$ subdivisions, with a discretization step length of the free leading-edge line vortices $\Delta x/C_0=0.06$ (i.e., with a step length/wing mesh length ratio $R=0.72$) and with free leading-edge and trailing-edge rolled-up wakes extending up to 0.5 of the wing root chord

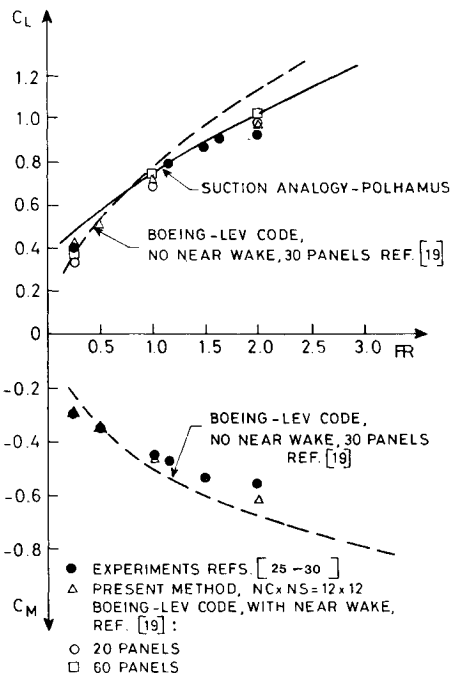

Fig. 4 Variation of the lift and pitching moment coefficients with the aspect ratio for flat-planform delta wings at $\alpha=20$ deg.

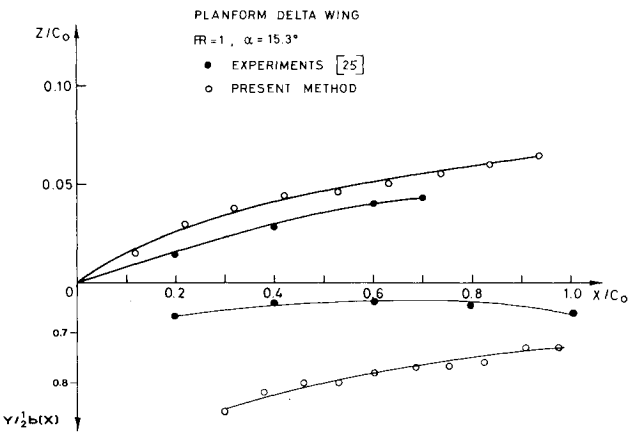

Fig. 5 Height of center of vorticity and vortex core path for a flat-planform delta wing, $\mathcal{R}=1$.

behind the wing trailing edge, terminating with semi-inifinite segment lines. These conditions are optimal for these calculations as determined in the parametric study which will be discussed later in the paper. The results obtained by the present paneling method are in very good agreement with the experimental data over the range of aspect ratios. At the higher aspect ratio, $\mathcal{R}=2$, the current method result for the lift coefficients is in good agreement with the Boeing-LEV code (with the near wake model) and is somewhat lower than the Polhamus suction-analogy result. These three methods predict higher lift coefficients than shown by the experimental data. Examination of the experimental results shows a loss in lift at higher angles of attack due to vortex bursting over the wing at the high angles. Experimental results of Wentz[29] show that, for a delta wing of $\mathcal{R}=2$, vortex breakdown appears over the wing at about $\alpha=18$ deg. The present method as well as the Boeing-LEV method and the suction-analogy method do not account for this phenomenon; therefore exact correlation with the experimental data for this wing at $\alpha=20$ deg is not possible.

The center of vorticity of the free line vortices at chordwise location X_j/C_0 is calculated by relation:

$$r_{c_i} = \sum_{i=1}^{N_j} \Gamma_i \cdot r_{i,j} \Big/ \sum_{i=1}^{N_j} \Gamma_i \tag{7}$$

where N_j is the number of free line vortices entering the cross plane at location X_j/C_0 and r_i is the position of the free line vortex Γ_i. For $X/C_0 > 1$, two summations are performed, one for the positive turning line vortices and the other for the negative ones. Figure 5 shows the calculated results for the height of center of vorticity above the wing chord plane Z_c/C_0 and its lateral position $Y_c/\frac{1}{2}b(x)$ as a function of the chordwise location X/C_0. Results are presented for a flat-planform delta wing of $\mathcal{R}=1$ at $\alpha=15.3$ deg. The experimental results of Peckham[25] for the position of the coiled vortex sheet cores as measured at a number of chordwise stations for the same wing and flow conditions are also presented. It is interesting to note that the position of the rotation center as calculated by Eq. (7) is similar to the position of the measured vortex core. Figure 6 shows the calculated results for the height of the center of vorticity as a function of the aspect ratio for $\alpha=20$ deg. As is seen from this figure, the center of vorticity moves farther away from the wing as the aspect ratio of the wing is increased.

Figure 7 shows the computed load coefficient distribution ΔC_p, calculated for a flat-planform delta wing of $\mathcal{R}=1$ at $\alpha=20.42$ deg, at three chordwise locations. Results are presented for three mesh spacings: 1) NC×NS = 12×12, i.e., 78 panels per half wing; 2) NC×NS = 15×15, i.e., 120 panels per half wing; and 3) NC×NS = 18×18, i.e., 171 panels per half wing. The results for $\mathcal{R}=1$ are compared with the experimental data of Hummel,[31] which were linearly interpolated to give the values at the same chordwise stations, obtained for a turbulent boundary layer. The general agreement between the calculated results and experimental data is quite good. Although it should be noted that the experiments of Hummel[31] on the flow over a delta wing of $\mathcal{R}=1$, which were carried out for a wide range of Reynolds numbers, have shown that the Reynolds number has no influence on the overall characteristics of the wing. However, the Reynolds number has quite a strong effect on the pressure distribution on the wing. Therefore we can expect only a qualitative agreement between the present potential results for the pressure distribution and the experimental measured data. The three-dimensional nonconical load distribution near the trailing edge is also well predicted by the present method, including the location of the vortex-induced pressure peak and the decrease of the load toward the trailing edge.

In some cases the calculations indicate the existence of a second peak just outboard of the main leading-edge vortex peak. Experimental results of Wentz,[28] Hummel, Hummel et al.,[32] Kirkpatrick,[30] Marseden et al.[33] and others, for delta wings at high angles of attack, clearly show the existence of a secondary vortex which occurs on the upper surface of the wing with its center located just outboard of the main vortex center, rotating in direction opposite to that of the leading-edge vortex. This secondary vortex is a result of the interaction of the vortices generated on the upper surface near the leading edge. The secondary vortex raises the suction near the leading edge, thereby generating a second peak. Although in the present calculation the flow over the wing (except at the leading edge) is assumed to be inviscid, the computed load distributions are similar to those of the real flow. Examination of the strengths of the line vortices embedded in the wing chord plane shows that the trailing line vortices on the wing chord plane are of opposite sign to that of the free leading-edge line vortices. At each cross section X/C_0 of the wing chord plane, the strengths of the trailing line vortices gradually increase toward the wing leading edge, up to about $0.8[b(x)/2]$, and then decrease quite rapidly toward the wing leading edge. The trailing line vortices that emanate from the wing at its trailing edge are also of opposite sign and rotate in the direction opposite to that of the free leading-edge line vortices. Releasing the trailing line vortices from the wing chord plane would probably generate a secondary vortex rotating in the opposite direction to the leading-edge vortex, with its center located just outboard of the main vortex center. On the other hand, the twin-peak distribution may be attributed to numerical stability problems in the computation of the leading-edge vortices trajectories that induce too high velocities on the wing surface at certain locations. However, the fact that this secondary flow appears in the velocity field calculations, as already indicated in Ref. 12, may be taken as an indication of the capability of this method to predict this phenomenon.

Results for Cambered Wings

Results are presented here for a symmetrical sharp leading-edge delta wing of $\mathcal{R}=1.15$ having a constant-percent camber at each airfoil section. The wing camber profiles are the NACA 230 mean lines designed for a section lift coefficient of $C_l=0.5$.[34] The resulting surface has a maximum

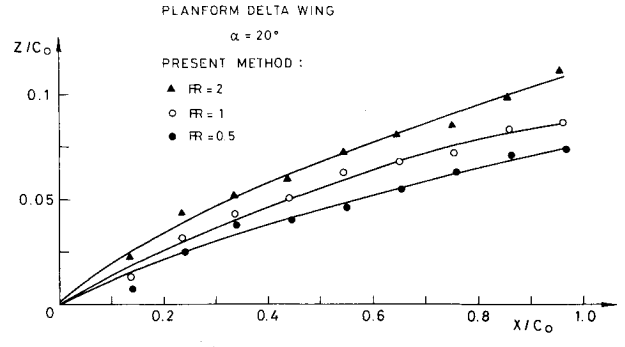

Fig. 6 Variation of height of center of vorticity path with aspect ratio for flat-planform delta wings at $\alpha=20$ deg.

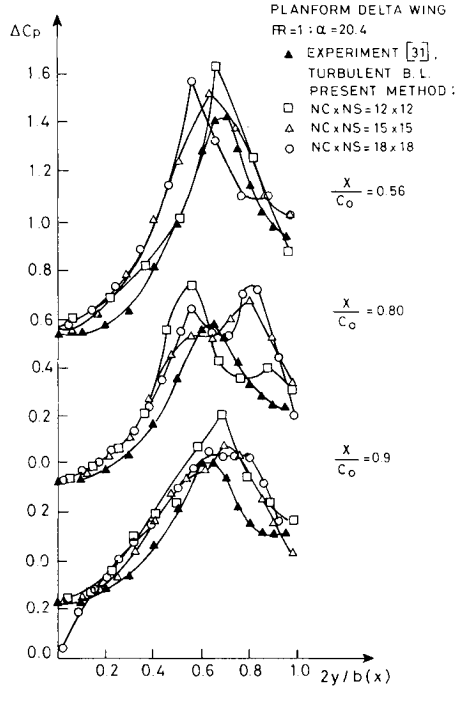

Fig. 7 Load coefficient distribution for a flat-planform delta wing with $\mathcal{R}=1$, at $\alpha=20.42$ deg.

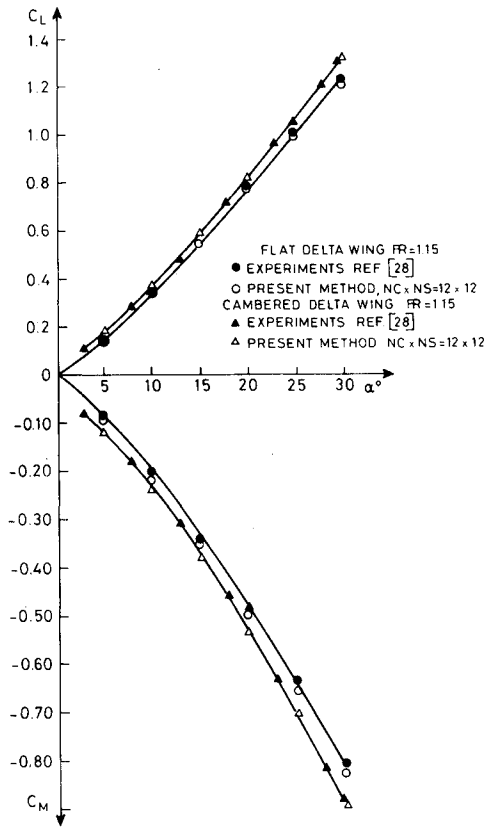

Fig. 8 Effect of wing camber on lift and pitching moment characteristics.

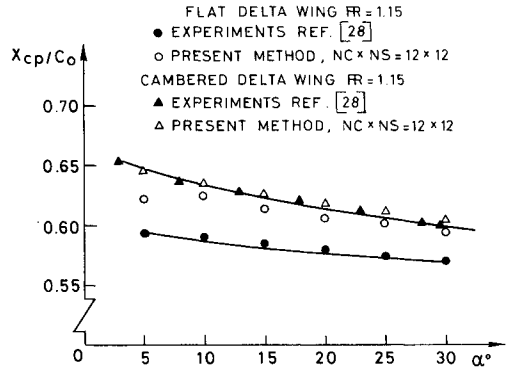

Fig. 9 Effect of wing camber on aerodynamic center of pressure.

camber at the apex, tapering to zero camber at the wing tips. The wing is illustrated in Ref. 23. The computed results are compared with the experimental results of Wentz[28] for the same wing. The results are also compared with the computed and the experimental results obtained for a flat-planform delta wing of the same aspect ratio.

Figures 8 and 9 present the computed results and the experimental data for the lift coefficient, pitching moment coefficient, and aerodynamic center of pressure, respectively, as a function of the angle of attack, for the cambered delta wing and its counterpart flat-planform delta wing. As seen from these figures, the computed results are in good agreement with the experimental data for both the cambered and uncambered delta wings. Comparisons of the results for the cambered wing with those of the flat-planform wing shows that the effect of cambering is to increase the lift coefficient and to produce a more negative pitching moment. The position of the aerodynamic center of pressure of the cambered wing is somewhat rearward compared with that of the flat-

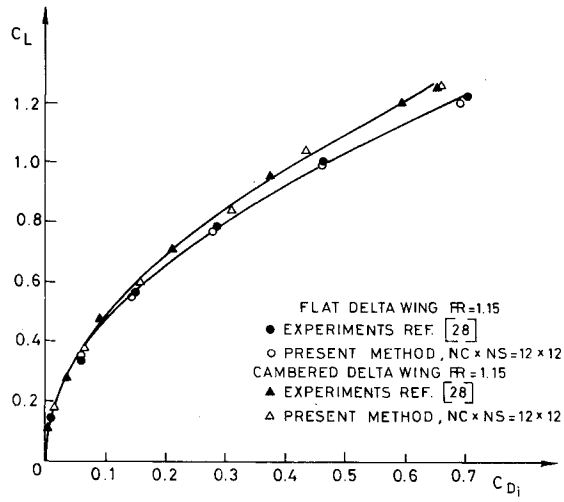

Fig. 10 Effect wing camber on drag coefficient.

planform wing. This indicates that the forward part of the wing suffers from a loss of lift, though the overall effect of cambering is to increase the lift. Similar trends were observed in the experiments of Wentz,[28] as shown in Figs. 8 and 9. Figure 10 shows the computed results and the experimental data of the induced drag coefficient as a function of the lift coefficient for both the cambered and the flat-planform delta wings. As seen from this figure, the effect of cambering is to reduce the induced drag coefficient. The computed result for the induced drag coefficient of the cambered wing is smaller than that of the flat wing by about 11% for $C_L = 1.2$. This result is in accordance with the experimental results. The reduction in the induced drag is due to the thrust component generated by the cambered leading edge of the wing.

Results for Thick Wings

The present method accounts for the thickness effects by superpositioning a panel source distribution obtained at zero incidence and set at an angle of attack on a vortex lattice laid out on a chord plane of the mean camber surface. This method is applicable only to small thickness and low cambered wings. In trial runs the vortex lattice was laid out on the thick wing surface to fulfill the correct boundary condition. This model resulted in extremely strong interaction between the vortices at the wing's leading edge, which caused divergence of the iterative procedure. Therefore, the present approximation, which does not fulfill the correct boundary condition for very thick cambered wings, is used.

Results are obtained for a symmetrical delta wing of $AR = 1$, having a 12% biconvex arc section at the centerline and a surface generated by radial straight lines from the tips. The wing is illustrated in Ref. 23. This wing has a constant biconvex shape with a constant thickness/chord ratio across the span. Results are also obtained for a planform delta wing of the same aspect ratio, $AR = 1$. The computed results are compared with the experimental results of Peckham[25] for these wings.

Figures 11 and 12 show the calculated and the experimental results for the lift coefficient, the pitching moment coefficient, and the aerodynamic center of pressure, respectively, as a function of the angle of attack α for the thick wing and its counterpart planform wing. The computed results are in very good agreement with the experimental data.

Comparsion of the results for the thick wing with those for the planform wing shows that the thickness causes a reduction in lift and a less negative pitching moment. The position of the center of pressure of the thick wing at high angles of attack is somewhat rearward compared to that of

the planform wing. This indicates that the greater portion of the loss of lift occurs over the forward part of the wing. Similar trends were also observed in the experiments of Peckham,[25] which are also shown in Fig. 12. Figure 13 shows the computed and the experimental results of the induced drag coefficient C_{D_i} as a function of the lift coefficient C_L for the thick wing. The drag due to lift coefficient of the planform wing, $C_L\tan\alpha$, is also shown. As is seen from this figure, the thick wing drag is lower than the $C_L\tan\alpha$ value. This result is due to the suction induced by the coiled vortex sheets (simulated by the vortex lines) acting on the forward sloping parts of the thick wing upper surface.

Figure 14 shows the calculated results for the height of the center of vorticity, Z_c/C_0, as a function of the chordwise location X/C_0, for the thick wing and for its counterpart planform wing. The experimental results of Z/C_0 of the cores of the coiled vortex sheet, measured at a numer of chordwise stations, are also shown in this figure. Comparison of the computed and experimental results for the thick wing with those of the planform wing shows that the center of vorticity of the thick wing is slightly farther away from the wing chord plane over the front and the central region of the wing.

Figure 15 presents the computed pressure coefficient distribution of the thick wing, obtained for $\alpha = 20.42$ deg at $X/C_0 = 0.73$. Results are presented for two mesh spacings: $NC \times NS = 12 \times 12$ and 15×15. This figure also presents the experimental pressure coefficient distribution obtained by Peckham[25] for the same wing and flow conditions. The present calculation does not predict the pressure peak near the leading edge of the wing as seen from the experimental data.

The Effects of Various Parameters on the Results

The sensitivity of the results to variations in the numerical parameters used in the computation method was studied.[23] The most efficient value for the initial inclination of the free line vortices was found to be $\alpha_0 = \alpha/2$ at zero yawing angle.

The computed results for three wake lengths $0.5C_0$, $1.0C_0$, and $2.0C_0$ are found to be practically identical. Therefore, in order to use less computing time, all calculations are computed with a rolled-up wake length of 0.5 root wing chord behind the wings' trailing edges followed by straight line extensions of the vortex wake downstream.

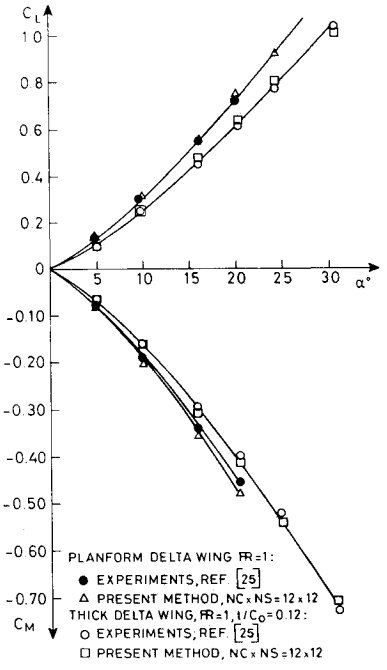

Fig. 11 Effect of wing thickness on lift and pitching moment characteristics.

Numerical experiments indicate that the suitable length of the free leading-edge line vortex segments should be between 0.25 and 1.0 of the length of the wing cells.

The effect of the number of panels on the lift coefficient, the pitching moment coefficient, and the center of pressure is presented in Fig. 16 for flat-planform delta wings of $\mathcal{R} = 1.0$ at $\alpha = 20$ deg. Similar results for $\mathcal{R} = 0.5$ and 2.0 are presented in Ref. 23. Denoting by R the ratio of the leading-

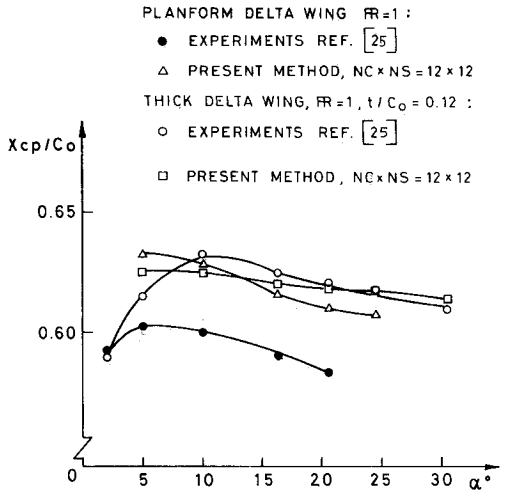

Fig. 12 Effect of wing thickness on the aerodynamic center of pressure.

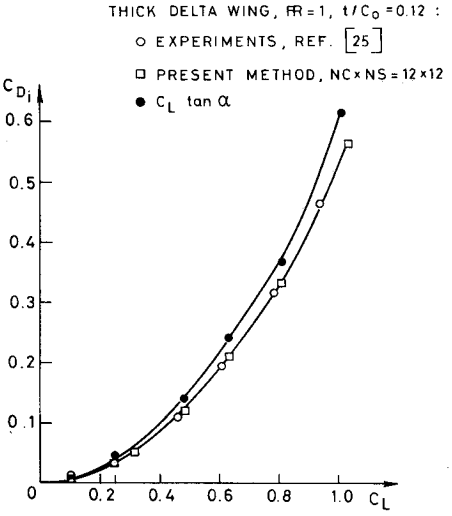

Fig. 13 Drag coefficient characteristics of the thick wing.

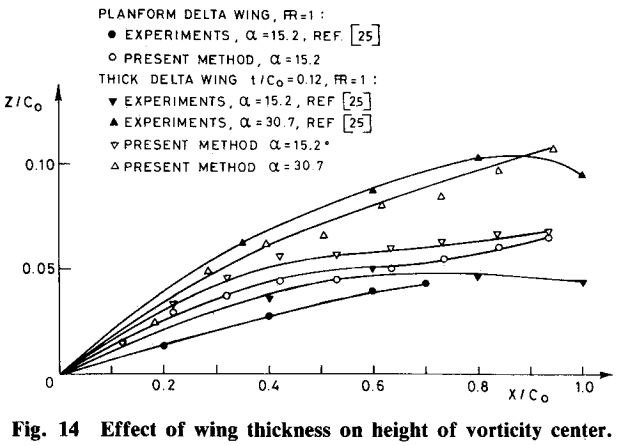

Fig. 14 Effect of wing thickness on height of vorticity center.

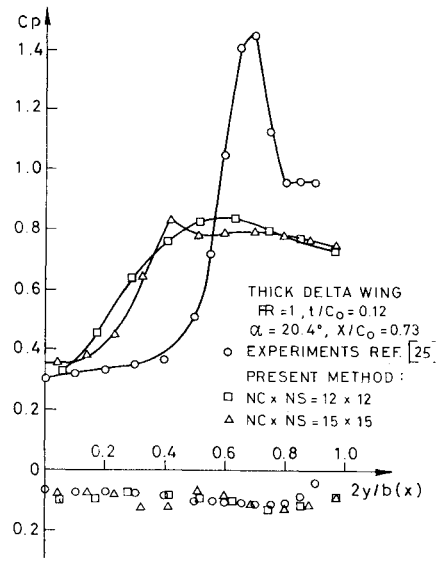

Fig. 15 Pressure coefficient distribution of thick wings at $x/C_0 = 0.73$.

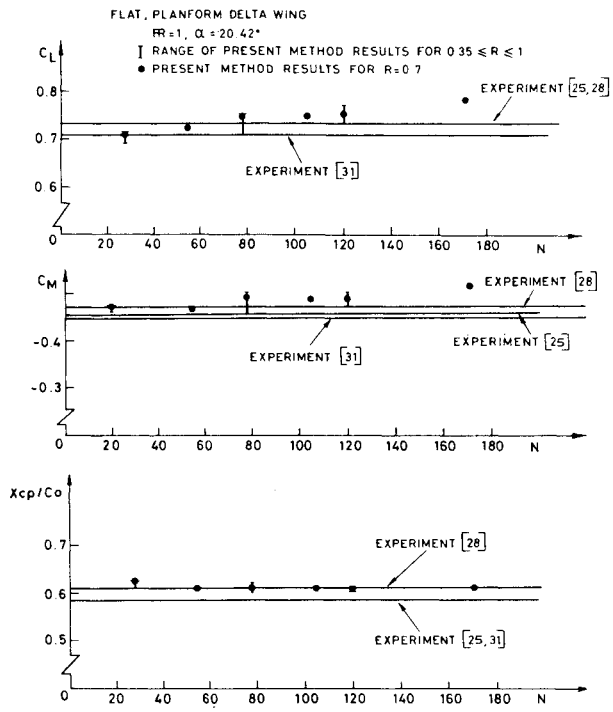

Fig. 16 Aerodynamic characteristics convergence with number of panels for a flat-planform delta wing with $\mathcal{R} = 1$ at $\alpha = 20$ deg.

edge line vortex segment length over the wing cell length, these figures show that the calculated aerodynamic coefficients converge for about 78 cells, namely, for NC × NS = 12 × 12. Figure 16 shows that at 171 cells there is a sudden loss of accuracy. This is probably caused by the accumulation of roundoff errors due to too many computations and by the erratic behavior that results from the increase in the number of free line vortices. Therefore, with the present cutoff distance using a limited number of divisions of the wing planform is recommended; 12 × 12 to 15 × 15 divisions are reasonable. It may be worthwhile to investigate the effects of varying the cutoff distance on this phenomenon.

Conclusions

The new vortex lattice model investigated in this work enables the calculation of the aerodynamic coefficients and the pressure distribution for planform and cambered delta wing over a wide range of aspect ratios. The calculated aerodynamic coefficients are found to be in very good agreement with experimental data. The pressure distribution calculation for these zero thickness wings is in reasonable agreement with experimental data. The good agreement is due to the special geometry of the horseshoe vortex element and the positioning of the control point in each cell, particularly in the triangular cells at the leading edges of a delta wing. Physically this model approximates the straight leading edge of the delta wing by a sawtooth-type leading edge. This model is applied to flat wings as well as cambered wings with very good results.

This model is also extended, in this work, to thick wings by adding panel-source distributions over the chord plane of the thickness configuration. Here again the calculated results for the aerodynamic coefficients simulate the experimental data very well. The calculated pressure distribution for thick wings, although indicating a secondary vortex separation near the trailing edge, does not predict the high-pressure peak found in the experiments of Ref. 25.

Since the accuracy of these calculations does depend on the particular selection of the various parameters in the numerical method, the sensitivity of the results and the convergence of the calculations are examined in a parametric study. This study shows that for reasonable values of the controlling parameters, the method enables reasonable convergence to a unique result.

A very significant improvement is achieved by the reduction of computing time. Here, by the use of the appropriate iteration procedures and computation techniques, the required computer time is reduced by an order of magnitude enabling calculations of wing characteristics in 2-20 min on an IBM 370/168 type computer.

The present method for the calculations of the aerodynamic characteristics of thin and thick wings can be combined with the calculations of the aerodynamic characteristics of bodies presented by Almosnino and Rom. Such a combined program should enable the evaluation of aerodynamic characteristics of wing-body configurations up to relatively high angles of attack.

Acknowledgments

The present research is based on the research programs sponsored in part by the U.S. Army under Grant DAERO-78-G119 and under U.S.A.F. Grant AFOSR-80-0064 through their European Research Offices, respectively.

References

[1]Polhamus, E. C., "A Concept of the Vortex Lift of Sharp Edge Delta Wings Based on a Leading-Edge Suction Analogy," NASA-TN D-3767, Dec. 1966.

[2]Margason, R. J. and Lamar, J. E., "Vortex-Lattice Fortran Program for Estimating Subsonic Aerodynamic Characteristics of Complex Planforms," NASA TN D-6142, Feb. 1971.

[3]Polhamus, E. C., "Application of the Leading-Edge-Suction Analogy of Vortex Lift to the Drag-Due-to-Lift of Sharp-Edge Delta Wings," NASA TN D-4739, Aug. 1968.

[4]Polhamus, E. C., "Prediction of Vortex Lift Characteristics by a Leading-Edge Suction Analogy," *Journal of Aircraft*, Vol. 8, April 1971, pp. 193-199.

[5]Mangler, K. W. and Smith, J. H. B., "A Theory of the Flow Past a Slender Delta Wing with Leading-Edge Separation," *Proceedings of the Royal Society of London*, Series A, Vol. 251, May 1959, pp. 200-217.

[6]Smith, J. H. B., "Improved Calculations of Leading-Edge Separation from Slender Delta Wings," RAE Tech. Rept. 66070, March 1966.

[7]Nagia, R. K. and Hancock, G. J., "A Theoretical Investigation for Delta Wings with Leading-Edge Separation at Low Speeds," Aeronautical Research Council, CP 1086, 1968.

[8]Rehback, C., "Etude numérique de nappes turbillonaires issues d'une ligne de décollement pres due bord d'attaque," *Recherche Aerospatiale, 1973-6*, 1973, pp. 325-330.

[9]White, R. P. Jr., "Wing-Vortex Lift at High Angles of Attack," AGARD-CP-204, Sept. 1976.

[10]Rom, J., Zorea, C., and Gordon, R., "On the Calculation of Non-Linear Aerodynamic Characteristic and the Near Vortex Wake," ICAS Paper 74-27, Aug. 1974.

[11]Zorea, C. R. and Rom, J., "The Calculation of Non-Linear Aerodynamic Characteristics of Wing and Their Wakes in Subsonic Flow," *20th Israel Annual Conference on Aviation and Astronautics*, Feb. 1978, pp. 36-48.

[12]Rom, J., Almosnino, D., and Zorea, C., "Calculation of the Non-Linear Aerodynamic Coefficients of Wings of Various Shapes and Their Wakes, Including Canard Configurations," *Proceedings of the 7th International Council of Aeronautical Sciences*, Vol. 1, Sept. 1978, pp. 333-334.

[13]Kandil, O. A., Mook, D. T., and Nayfeh, A. H., "Nonlinear Prediction of the Aerodynamic Loads on Lifting Surfaces," *Journal of Aircraft*, Vol. 13, Jan. 1976, pp. 22-28.

[14]Kandil, O. A., Mook, D. T., and Nayfeh, A. H., "A Numerical Technique for Computing Subsonic Flow Past Three-Dimensional Canard-Wing Configurations with Edge Separations," AIAA Paper 77-1, 1977.

[15]Kandil, O. A., Atta, E. H., and Nayfeh, A. H., "Three Dimensional Steady and Unsteady Asymmetric Flow Past Wings of Arbitrary Planforms," AGARD-CP-227, Sept. 1977.

[16]Weber, J. A., Brune, G. W., Johnson, F. T., Lu, P., and Rubbert, P. E., "Three-Dimensional Solution of Flows Over Wings with Leading Edge Vortex Separation," *AIAA Journal*, Vol. 14, April 1976, pp. 519-525; see also NASA CR 132709 and 132710, 1975.

[17]Johnson, F. T., Lu, P., Brune, G. W., Weber, J. A., and Rubbert, P. E., "An Improved Method for the Prediction of Completely Three-Dimensional Aerodynamic Load Distribution on Configurations with Leading-Edge Separation," AIAA Paper 76-417, 1976.

[18]Hoeijmakers, H. W. M. and Bennekers, B., "A Computational Method for the Calculation of the Flow About Wing with Leading Edge Vortices," Paper 25, AGARD-CP-247, Jan. 1979.

[19]Johnson, F. T., Tinoco, E. N., Lu, P., and Epton, M. A., "Three-Dimensional Flow Wings with Leading-Edge Vortex Separation," *AIAA Journal*, Vol. 18, April 1980, pp. 367-380.

[20]Johnson, F. T., Lu, P., Tinoco, E. N., and Epton, M. A., "An Improved Panel Method for the Solution of Three-Dimensional Leading-Edge Vortex Flows," NASA CR-3278, July 1980.

[21]Smith, J. H. B., "Inviscid Fluid Models, Based on Rolled-Up Vortex Sheets, for Three-Dimensional Separation at High Reynolds Number," *AGARD Lecture Series, No. 94, On Three-Dimensional and Unsteady Separation at High Reynolds Numbers*, Paper 9, Feb. 1978.

[22]Woodward, F. A., "An Improved Method for the Aerodynamic Analysis of Wing-Body-Tail Configuration in Subsonic and Supersonic Flow," NASA CR-2228, May 1973.

[23]Gordon, R. and Rom, J., "Calculation of Aerodynamic Characteristics of Wings with Thickness and Camber by a New Method Based on the Modified Vortex Lattice Method," Aeronautical Engineering Technion—Israel Institute of Technology, TAE No. 493, July 1982.

[24]Jordan, H. L. et al, Memorandum "Uber zukünftige nationale Zusammenarbeit in der Strömungforschung, insbesondere der Aerodynamik auf dem Gebeit der Strömungen mit Ablösung," Cologne, FRG, Oct. 1979.

[25]Peckham, D. H., "Low-Speed Wind-Tunnel Tests on a Series of Uncambered Slender Pointed Wings with Sharp Edges," Aeronautical Research Council, RM 3186, 1961.

[26]Bartlett, G. E. and Vidal, R. J., "Experimental Investigation of Influence of Edge Shape on the Aerodynamic Characteristics of Low Aspect Ratio Wings at Low Speeds," *Journal of the Aeronautical Sciences*, Vol. 22, Aug. 1955, pp. 517-533.

[27]Fox, C. H. Jr. and Lamar, J. E., "Theoretical and Experimental Longitudinal Aerodynamic Characteristics of an Aspect Ratio 0.25 Sharp-Edge Delta Wing at Subsonic, Supersonic and Hypersonic Speeds," NASA TN D-7651, Aug. 1974.

[28]Wentz, W. H., "Effects of Leading-Edge Camber on Low-Speed Characteristics of Slender Delta Wings," NASA CR-2002, 1972.

[29]Wentz, W. H. Jr. and Kohlman, D. L., "Vortex Breakdown on Slender Sharp-Edged Wings," *Journal of Aircraft*, Vol. 8, March 1972.

[30]Kirkpatrick, D. L. I., "Analysis of the Static Pressure Distribution in a Delta Wing in Subsonic Flow," Aeronautical Research Council RM 3619, 1970.

[31]Hummel, D., "On the Vortex Formation over a Slender Wing at Large Angles of Incidence," Paper No. 15, AGARD-CP-247, Jan. 1979.

[32]Hummel, D. and Redeker, G., "Experimentelle Bestimmung der Gebundenen Wirbellinien Sowie des Strömungsverlaufs in der Umgebung der Hinterkante eines schlanken deltaflügels," *Abhandlungen der Braunschweigischen Wissenschaftlichen Gesellechaft*, 22, 1972, pp. 273-290.

[33]Marsden, D. J., Simpson, R. W., and Rainbird, W. J., "An Investigation into the Flow Over Delta Wings at Low Speeds with Leading Edge Separation," Aeronautical Research Council, Cranfield, England, UK, Rept. 114, ARC 20409, Feb. 1958.

[34]Abbott, I. H. and Van Doenhoff, A. C., "Theory of Wing Sections," Dover, New York, 1958.

[35]Almosnino, D. and Rom, J., "Calculation of Symmetric Vortex Separation Affecting Subsonic Bodies at High Incidence," *AIAA Journal*, Vol. 21, March 1983, pp. 398-406.